CrossMark

Automated Segmentation and Quantification of Drusen in Fundus and Optical Coherence Tomography Images for Detection of ARMD

Samina Khalid[1,2] · M. Usman Akram[3] · Taimur Hassan[3,4] · Amina Jameel[5] ·
Tehmina Khalil[1,2]

Abstract

Age-related macular degeneration (ARMD) is one of the most common retinal syndromes that occurs in elderly people. Different eye testing techniques such as fundus photography and optical coherence tomography (OCT) are used to clinically examine the ARMD-affected patients. Many researchers have worked on detecting ARMD from fundus images, few of them also worked on detecting ARMD from OCT images. However, there are only few systems that establish the correspondence between fundus and OCT images to give an accurate prediction of ARMD pathology. In this paper, we present fully automated decision support system that can automatically detect ARMD by establishing correspondence between OCT and fundus imagery. The proposed system also distinguishes between early, suspect and confirmed ARMD by correlating OCT B-scans with respective region of the fundus image. In first phase, proposed system uses different B-scan based features along with support vector machine (SVM) to detect the presence of drusens and classify it as ARMD or normal case. In case input OCT scan is classified as ARMD, region of interest from corresponding fundus image is considered for further evaluation. The analysis of fundus image is performed using contrast enhancement and adaptive thresholding to detect possible drusens from fundus image and proposed system finally classified it as early stage ARMD or advance stage ARMD. The proposed system is tested on local data set of 100 patients with 100 fundus images and 6800 OCT B-scans. Proposed system detects ARMD with the accuracy, sensitivity, and specificity ratings of 98.0, 100, and 97.14%, respectively.

Keywords Optical coherence tomography (OCT) · Fundus images · Age related macular degeneration (ARMD) · RPE · Grading

Introduction

Age-related macular degeneration (ARMD) is a degenerative eye disease that affects the macular region due to the formation of drusen in Bruch's membrane in the basement of RPE layer and cause deformation and thickening of RPE layer [1]. It mostly occurs in aged persons after 60 years, but can also occur earlier. ARMD can cause severe visual impairments and if it is not treated at an early stage, it can result in an irreversible loss of central vision. After age, patients with diabetes, cardiovascular disease, and genetic susceptibility are also at risk of having ARMD disorder [2, 3]. In EUREYE study, there is a found positive association in patients of diabetes with neovascular ARMD [4]. Therefore, diabetic patients are at high risk of having wet ARMD disorder. World Health Organization (WHO) mentioned in their report that a high rate of people suffers from diabetes and cardiovascular diseases in Pakistan [3]. ARMD is also a threatening disease in developed countries like United States of America (USA) and around 40% elderly population in USA is suffering from ARMD [5]. These degenerative retinal disorders are expected to be doubled in next 25 years [6]. Clinically, drusens are the main source of ARMD, which cause hyperpigmentation of RPE. Shape of RPE is deformed due to presence of drusens. Appearance of these drusens in macular region causes a central vision distortion. Many researchers have proposed fully automated systems

✉ M. Usman Akram
usmakram@gmail.com

1   Department of Computer Science & Information Technology, Mirpur University of Science and Technology, Mirpur, Pakistan

2   Department of Software Engineering, Bahria University, Islamabad, Pakistan

3   Department of Computer Engineering, National University of Sciences and Technology, Islamabad, Pakistan

4   Department of Electrical Engineering, Bahria University, Islamabad, Pakistan

5   Department of Computer Engineering, Bahria University, Islamabad, Pakistan

for the detection of drusen from color fundus photographs. Although fundus photography gives gold standards for detecting drusen pathology; nevertheless, fundus imaging is found to be quite feeble for the early localization and quantitation of drusen, due to the varying nature of macular pathology especially in early stages [7]. Therefore, all the automated self-diagnosis system to detect ARMD from fundus imaging are less sensitive to early pathological conditions of ARMD. Optical coherence tomography (OCT) is one of the latest advancements in ophthalmic imaging. OCT provides a reliable and objective visualization of cross-sectional drusen pathology. Spectral domain optical coherence tomography (SD-OCT) provides high resolution OCT imagery as compared to time domain optical coherence tomography (TD-OCT) [8].

Many researchers have worked on the diagnosis of drusen pathology from fundus images. However, only a few good studies have been carried out on automated diagnosis of ARMD using OCT. Z. B. Sbeh et al. [9], proposed a method for segmentation of angiographic eye fundus images in order to extract drusens, yellowish deposits at the retina level, using an adaptive algorithm based on mathematical morphology transforms. Z. B. Sbeh et al. [10] also presented a novel segmentation method based on their proposed transformation technique which involved the search for a new class of regional maxima components of the image. K. Rapantzikos et al. [11, 12] developed a novel segmentation technique which is the histogram-teased adaptive local thresholding (HALT) to detect drusens in fundus images by extracting the useful information without being affected by the presence of other pathological structures. Apart from this, different fuzzy logic-based techniques [13–15] and texture-based methods [16–18] have been proposed for drusens detection and segmentation from fundus images. L. Brandon et al. [19] used a multi-level approach, starting from the classification at the pixel level and then to the region level, area level, and finally to the image level which allowed to gather the lowest level of details for possible detection of drusens. They achieved the accuracy of 87% on the dataset containing 119 fundus images.

ARMD detection at an early stage is important and OCT imagery provides an objective and reliable visualization of macular pathology [20], particularly identification and quantification of drusens. Figure 1 depicts the correspondence between fundus and OCT retinal images for both healthy and ARMD pathology while Fig. 2 relates the appearance of drusen on fundus image with RPE atrophic profile in OCT brightness scan (B-scan).

In ARMD-effected eye, RPE layer is displaced and deformed due to extracellular material deposits located between the basal lamina of RPE and the inner collagenous layer of Bruch's membrane [21]. Various clinical studies have been presented with the detailed analysis on the diagnosis of ARMD but only few automated systems exist that provide the detection of ARMD pathology from OCT scans. N. Jain et al. [22] have performed comparative analysis to elaborate

effectiveness of OCT over fundus images to detect drusen and argued that OCT imagery offers greater accuracy in providing details regarding border of hard and soft drusens than inspection of fundus images. Their studies have proved that drusen area and size measurement correlates with disease progression in dry ARMD. S. J. Chiu et al. [23] proposed an algorithm to segment three retinal boundaries efficiently as compared to that of manual segmentation by graders. They have tested their proposed algorithm on the dataset of 220 B-scans of 20 patients. S. Farsiu et al. [24] have defined quantitative indicators (QI) to detect drusen that cause intermediate ARMD from OCT images. QI's that were considered by them includes total retina (TR) volumes, RPE drusen complex (RPEDC) volumes, and abnormal RPEDC thickening and thinning volumes. They have used a dataset of 384 subjects including 115 images of elderly subjects without ARMD and 269 images with intermediate ARMD, which is up till now the largest quantitative OCT dataset containing RPE thickness profiles and its abnormalities. Abnormal RPEDC thickness QI was found as the single most useful feature that can be used to detect intermediate ARMD. In SD-OCT images, accurateness of anatomical structures is critical for the diagnosis and analysis of ocular diseases [25]. Most of commercially available OCT systems are used to quantify retinal thickness profiles. Some of these systems are also used to measure the retinal nerve fiber layer (RNFL) thickness [26]. Automated analysis of OCT images is an active field of research with intentions to speed up screening of patients and to enable remote identification of retinal diseases [27]. J. Y. Lee, et al. [28] presented novel segmentation framework that is used to segment retinal layers from diabetic macular edema (DME)-affected OCT images, acquired from cirrus and spectralise system.

G. M. Somfai, et al. [29] calculated different structural and optical features from cross-sectional retinal pathology using OCT imagery to diagnose healthy and diabetic eyes with mild or no mild retinopathy. Q. Chen et al. [30] presented an automated drusen segmentation method for SD-OCT retinal images, which leverages a priori knowledge of normal retinal morphology and anatomical features. D. C. Fernández et al. [31] proposed model-based enhancement segmentation approach with the combination of complex diffusion filtering with coherence enhancing diffusion filtering for de-noising, segmentation, and structural analysis in OCT retinal images and their proposed approach gives good performance for noise removal and enhancement of retinal layers from OCT images. S. J. Chiu et al. [32] presented a fully automated system for segmentation of retinal layered structure using OCT images by applying graph-cut theory and dynamic programming (GTDP) approach that significantly lessen processing time of segmentation and features extraction. An improved version of [32] based on kernel regression (KR) method was proposed [33] to improve the segmentation of
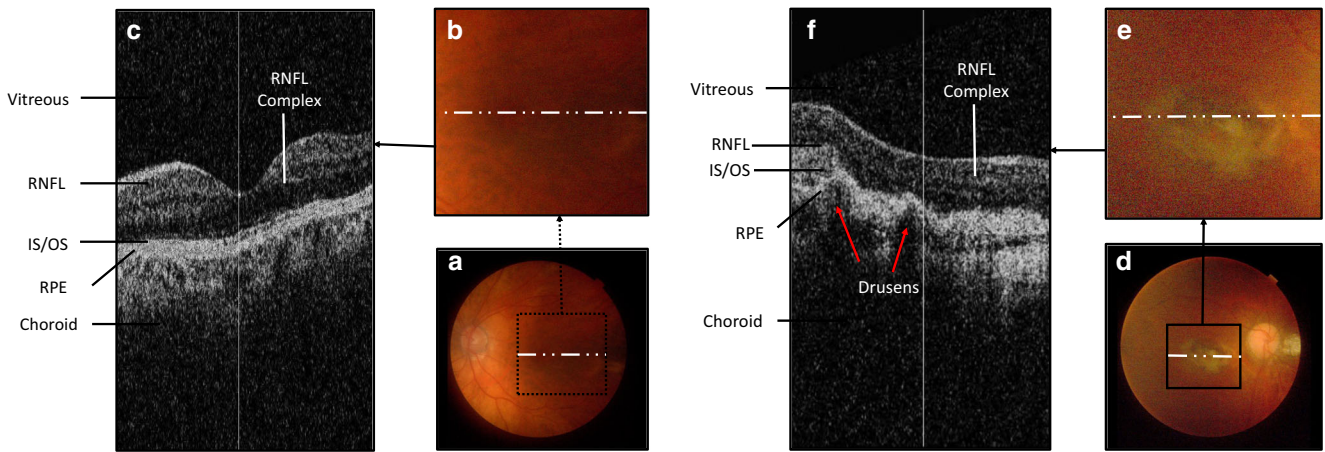
Fig. 1 (a) Fundus image of a normal retina. Black square represents the macular region of normal retina, whose cross-sectional pathology is presented by SD-OCT scan in (c), (b) summed voxel projection (SVP) image of normal retina, (c) SD-OCT B-scan directed by the white dashed dotted line in (b), (d) fundus image of the ARMD-effected retina. Black square represents the macular region of ARMD retina, whose cross-sectional pathology is presented in (f), (e) SVP of ARMD-effected retina shown by white dashed-dotted line, and (f) ARMD-effected SD-OCT B-scan

retinal layers boundaries with the combination of previously developed GTDP framework. Apart from this, Table 1 gives an overview of some of the automated methods that have been proposed for the diagnosis of ARMD from OCT images. OCT imagery-based clinical decision support systems provide advancement towards drusen quantification. However, there are some challenges which need to be addressed for reliable drusen quantification. One of the challenges is the estimation of RPE layer where drusen appears. In low quality OCT images, the accurate segmentation of RPE layer can be cumbersome even from normal B-scan, as inner segment/outer segment (IS/OS) layers are frequently merged with RPE layer. In [34], it presented an application software interface which is used to manually identify different retinal layers from macular and ocular pathology.

Fig. 2 (a) Fundus image of ARMD-effected retina, (b) macular region of (a) depicting the drusen pathology, (c) SD-OCT scan of oval shaped area in (b), red dashed line directs the location of B-scan of image presented (b) showing some small drusen, (d) SD-OCT scan from a circular area in (b) red dashed line directs the location of B-scan of image presented in (b), showing various small drusen
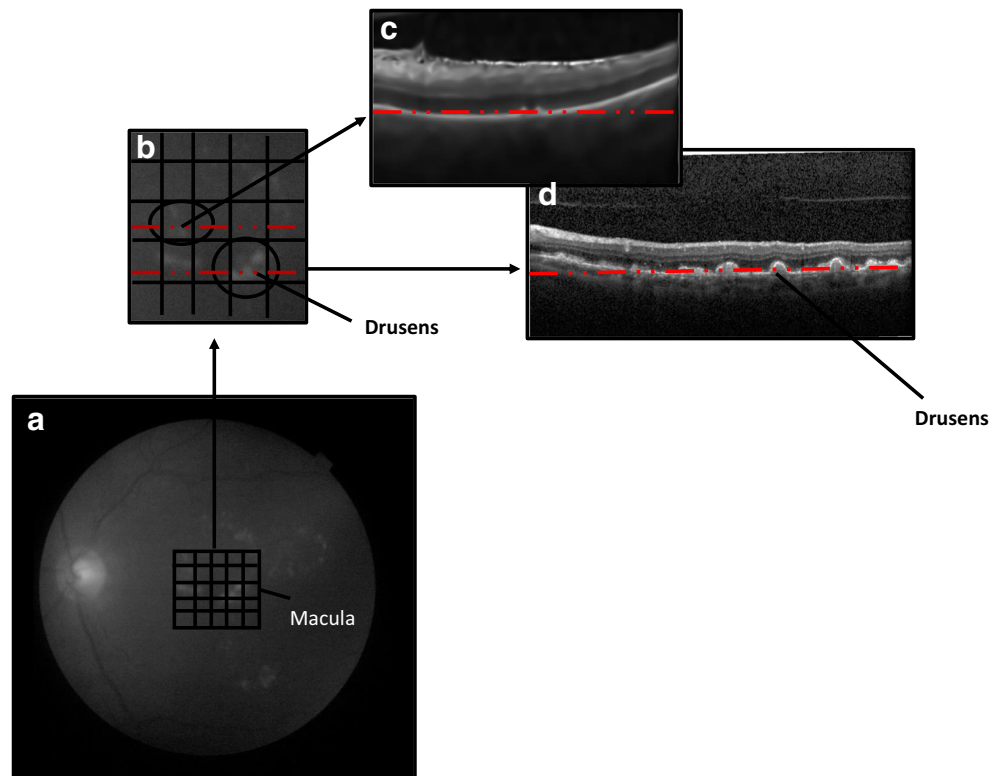
Table 1 OCT-based clinical decision supported systems used for retinal layer segmentation

Authors	Method used for retinal layers segmentation	Dataset
A. M. Bagci et al. [33]	Gray level mapping, edge detector operator	10 normal images
S. J. Chiu et al. [34]	Kernel regression and GTDP (graph theory + dynamic programming)	110 B-scans DME images
F. Rossant et al. [35]	Diffusion filter, Markov random field, K-mean clustering	25 normal, 47 diseased images
Q. Yang et al. [36]	Canny edge, dynamic programming	19 glaucoma images (left and right eyes)
A. Yazdanpanah et al. [37]	Chan-Vese energy-minimizing active contour	–
G. R. Wilkins et al. [38]	Median filter, bilateral filter, thresholding, and boundary detection algorithm	16 patients effected with macular edema
Y. Huang, et al. [39]	Canny edge operator	4 normal and 24 diabetic macular edema (DME) images
R. Kafieh et al. [40]	Graph-based segmentation	Normal images
A. M. Abhishek et al. [41]	Median filter, method I. Canny edge detection filter, LOG filter, method II. Graph theory	DME Images

Contributions

Most of the automated systems that have been proposed in literature are based on fundus images which are less sensitive to early pathological conditions of ARMD. Very few automated systems exist which uses OCT imagery for the early diagnosis of ARMD.

In this paper, we propose fully automated decision support system for the diagnosis of ARMD by establishing the correspondence between both retinal fundus and OCT imagery. The significant scientific contributions of the proposed system are summarized below:

- This paper presents clinical decision support system for the automated diagnosis of ARMD by establishing the correspondence between both fundus and OCT imagery.
- The proposed system is a fully automated system that distinguishes ARMD-affected patients from the early ARMD suspects. This has been established by correlating degenerative pathology in both fundus and OCT imagery.
- Furthermore, the proposed system reconstructs a complete 3D RPE surface from OCT volumetric scans, which can be mapped onto the respective fundus image to validate the detected drusen.
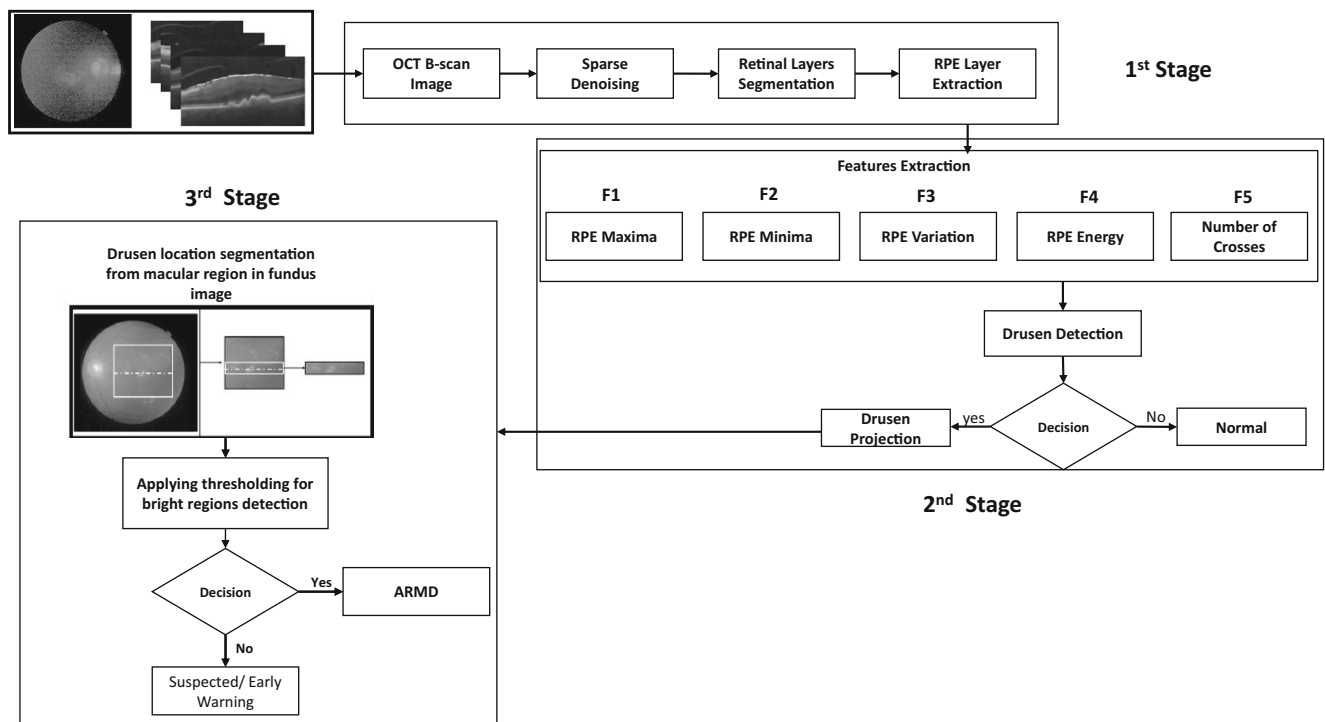
Fig. 3 Flow diagram of proposed automated system showing different stages for the detection and grading of ARMD

Table 2   Dataset used

Imagery	Total	Healthy	ARMD	
			Early	Advanced
OCT scans	6800	4760	476	1564
Fundus	100	70	7	23

Proposed Methodology

We propose a fully automated self-diagnosis system that is based on three major stages. The first stage of the proposed system is related to acquiring fundus and OCT volumetric scan. From OCT volumetric scan, each B-scan is processed to extract its RPE atrophic profile which is then used to reconstruct a complete 3D RPE surface. The second stage of the proposed system is related to extracting five distinct features from the segmented RPE layer and classifying the candidate subject as healthy or ARMD suspect based on the analysis of OCT profile. In case of suspect ARMD, proposed algorithm proceeds to third stage where surrounding region against suspected B-scan is extracted from corresponding fundus image and algorithms are applied for possible drusen detection. Based on the results from third stage, patient is finally diagnosed as early or advanced ARMD. Figure 3 depicts the block diagram of the proposed system.

Dataset Description

There is no online dataset available which provides both OCT and fundus images for ARMD analysis. We have used a custom dataset in this research which is acquired from armed forces institute of ophthalmology (AFIO). The dataset was annotated by two expert ophthalmologists from AFIO. A subset of 100 patients has been selected for which both experts gave same labeling. They labeled the images as normal and with ARMD and further divide ARMD into early or advanced. All those cases which show some signs of ARMD in OCT volumes but no such sign on fundus image are labeled as suspected/early ARMD. The dataset is captured from spectralise SD-OCT imaging camera with 68 scans per patient. The manufacturer of spectralise SD-OCT machine is Heidelberg Engineering Inc. Table 2 shows the detailed description about the used dataset. The dataset is available at www. biomisa.org/armd. As mentioned earlier and shown in Fig. 3, proposed technique have three phases which are explained below.

RPE Layer Extraction (Stage-1)

First phase of proposed system is to perform de-noising and to extract RPE layer from input OCT B-scan. Previously, we have proposed systems to extract retinal layers from OCT B-scans [42] and used them to reconstruct retinal surfaces [43] for detection of macular edema (ME) and central serous retinopathy (CSR). In [42, 43], we have also described the complete mathematical models of our proposed system in detail and same have been used here for extraction of RPE layer.

Figure 4 shows segmented layers including RPE layer using methods proposed in [42, 43]. Out of these segmented layers, RPE layer is automatically selected which shows the atrophic degenerative profile for that respective B-scan.

RPE Layer Analysis (Stage-2)

Second phase of proposed system is analysis of RPE layer which is based on two submodules feature extraction and classification.
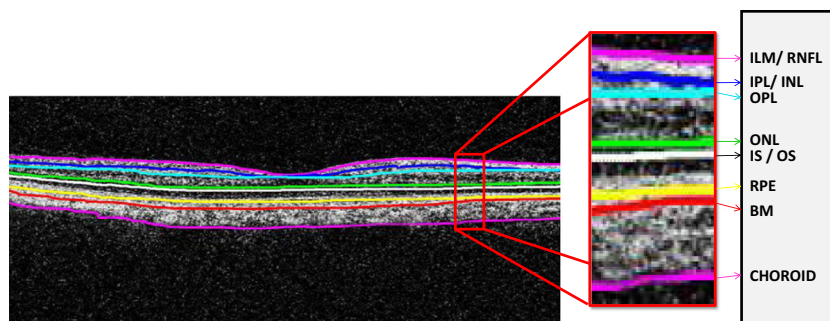
Fig. 4   Segmented retinal layers in one A-scan: inner limiting membrane (ILM), retinal nerve fiber layer (RNFL), inner plexiform layer (IPL), inner nuclear layer (INL), outer nuclear layer (ONL), outer plexiform layer (OPL), outer segment (OS), inner segment (IS), RPE, and Bruch's membrane (BM) and choroid

Fig. 5 **a** RPE layer is shown in yellow color with drusens. Segmented ILM is shown in red color and choroid is shown in green color, **b** zero-crossings are highlighted by red circles
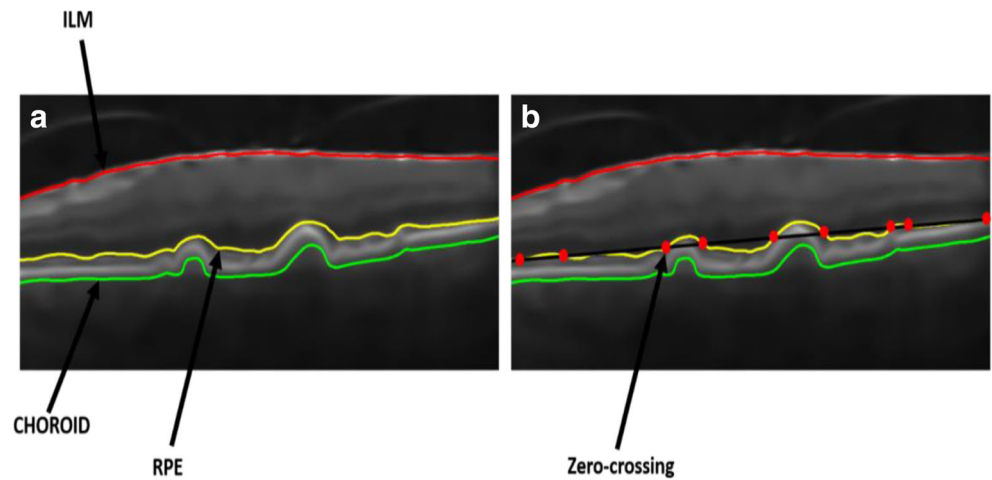
Feature Extraction

After extracting RPE layer ($R(x, y)$) from OCT scans, five distinct features are obtained which are further used to classify subjects as normal or early ARMD affected. The detailed description of each feature is given below:

RPE Maxima (F_1): This feature represents the maximum peak value in RPE layer as expressed in Eq. (1):

$$F_1 = \text{Max}\left[R(x,y)\right] \tag{1}$$

RPE Minima (F_2): Its minimum value in RPE layer, and is expressed in Eq. (2):

$$F_2 = \text{Min}\left[R(x,y)\right] \tag{2}$$

RPE Variation (F_3): In this feature the variation in RPE layer is computed and illustrated by Eq. (3):

$$F_3 = |F2 - F1| \tag{3}$$

RPE Energy (F_4): The total energy within the RPE surface is obtained through Eq. (4):

$$F_4 = \left(\sum_{r=0}^{n-1} |R_D(r)|^2\right) \tag{4}$$

Number of Crosses (F_5): This feature measures the amount of zero crossings on RPE layer. In order to measure this, a first order Lagrange polynomial is automatically fitted onto extracted RPE layer. Zero crossing is that

point where the fitted polynomial equates the original RPE layer as depicted in Eqs. (5)–(9).

$$L_{N,j}(x) = \prod_{m=0,m\neq j}^{N} \frac{(x-x_m)}{(x_j-x_m)} \tag{5}$$

$$R'(x) = \sum_{k=0}^{N} f(x_k) L_{N,k}(x) \tag{6}$$

$$Z_C(x) = \sum_{k=0}^{L} |\{i \epsilon\{1, 2, \ldots, n\} : \delta_i = \mathbb{Z}\}| \tag{7}$$

$$\mathbb{Z} = \left\{R(x) - R'(x)\right\} : \rightarrow 0 \tag{8}$$

$$F_5 = \left(\sum_{x_i=0}^{n-1} Z_C(x_i)\right) \tag{9}$$

Table 3 Feature vectors from five randomly selected subjects from healthy and ARMD patients

Type	Features				
	F1 (mm)	F2 (mm)	F3 (mm)	F4	F5
Healthy	1.20	− 0.36	1.56	24.070	2.00
	0.87	− 0.80	1.67	29.060	1.00
	0.80	− 0.57	1.37	26.008	1.00
	4.00	− 2.56	6.56	68.206	2.00
	0.93	− 0.36	1.29	32.036	3.00
Mean	1.56	− 0.93	2.49	35.87	1.80
Std	1.37	0.92	2.28	18.32	0.83
ARMD	10.93	− 1.20	12.13	118.47	10
	13.08	− 1.64	14.72	207.68	9
	16.48	− 5.60	22.08	439.89	15
	11.37	− 2.35	13.72	140.38	12
	11.93	− 0.88	12.81	106.29	16
Mean	12.75	− 2.33	15.09	202.54	12.4
Std	2.23	1.90	4.02	138.34	3.04
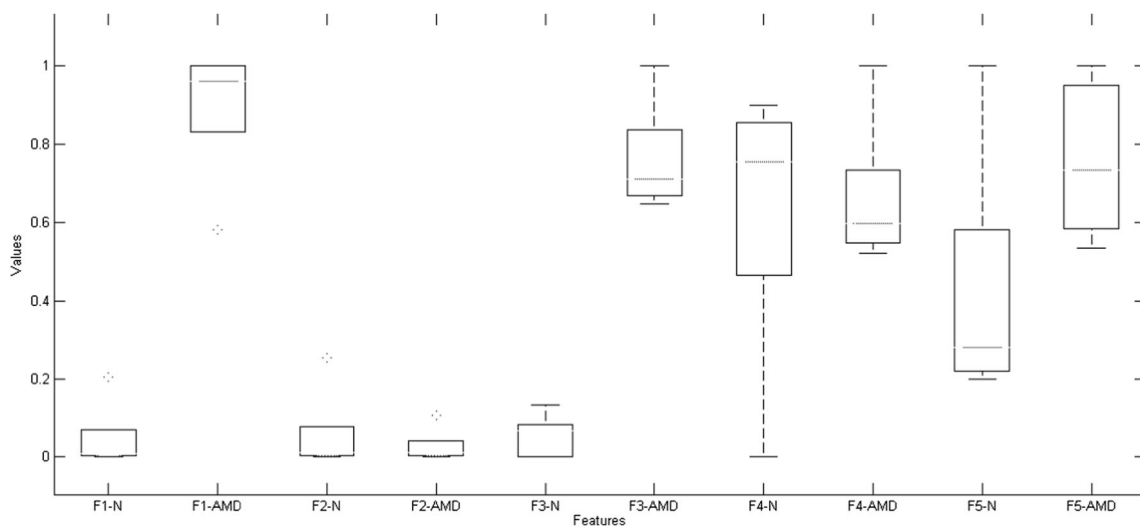
Fig. 6 Box plots for each feature. Here, feature number, "N" shows value distribution of feature for healthy class whereas feature number, "AMD" shows same for ARMD cases

where N represents the order of the fitted polynomial which is 1 is our case, $R(x)$ is the original B-scan of RPE layer, $R'(x)$ is the approximated first order Lagrange polynomial, $\nexists$ represents the intersection point of $R(x)$ and $R'(x)$, and $Z_C(x)$ represents the occurrence of zero crossings in single B-scan of RPE layer. The difference between $R(x)$ and $R'(x)$ is considered to be a zero-crossing point if its margin is less than 10^{-20}. This is to avoid extra zero-crossings. Figure 5 depicts the number of zero-crossings which are extracted from the

randomly selected ARMD positive B-scan. Table 3 shows five distinct features for the five randomly selected subjects from both categories. These five features are used to determine the candidate subject as healthy or ARMD using OCT image. It also shows mean and standard deviation values of these features to describe per class behavior of each feature with its variation. Figure 6 shows complete distribution of all five features for the whole dataset for healthy and ARMD cases in form of box plots.
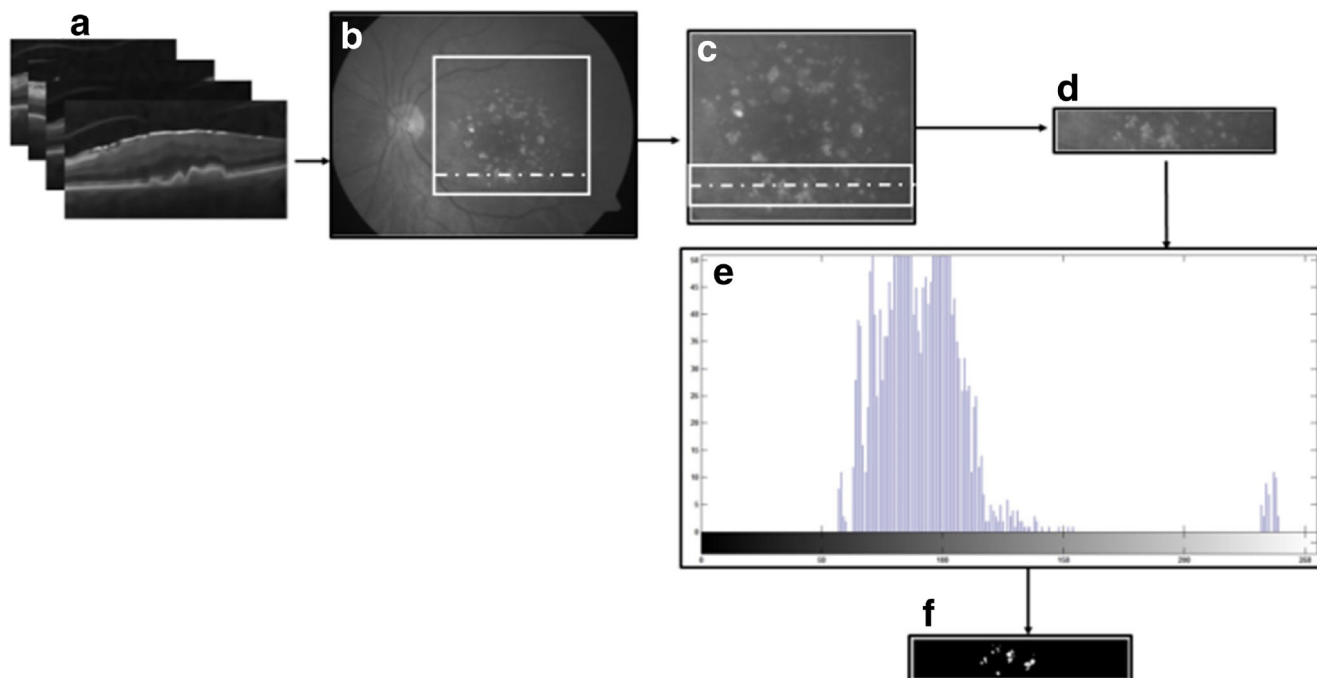
Fig. 7 Drusen extraction from the candidate fundus image (a) OCT B-scans (b) macular region corresponding to suspect OCT B-scan, (c) region of interest across location of suspected OCT B-scan (d) segmented bright lesions highlighted in (c), (d) cropped region of interest (e) probability mass function of (c), (f) digitalized binary map $B_{\text{Fundus}}(x, y)$ indicating the segmented drusen

Table 4 Proposed system performance

AFIO dataset	Type	Correctly classified/total	Accuracy (%)	Sensitivity (%)	Specificity (%)
OCT image analysis					
B-scans	Normal	4579/4760	96.4	97.1	96.19
	ARMD	1981/2040			
Patients	Normal	68/70	98.0	100	97.14
	ARMD	30/30			
Fundus images analysis					
Patients	Normal	63/70	86.0	76.6	90.0
	ARMD	23/30			
Fusion (combined images analysis)					
Patients	Normal	68/70	98.0	100	97.14
	ARMD	30/30			

Classification

The proposed system implements support vector machine (SVM) based classification system for detection of ARMD pathology [44]. The proposed system uses radial basis function (RBF) along with SVM to handle nonlinear distribution of data. After extracting five distinct features from the input OCT B-scan, they are used to classify subject as normal or suspect ARMD. If the candidate is classified as healthy then fundus image analysis is skipped. This is because if there are no abnormal ARMD symptoms found on RPE layer in OCT image then the respective fundus scan will be normal as well. But if the candidate is classified as having ARMD symptoms then the proposed classification system considers it as suspect case and further confirms whether it is an early warning or the subject is really suffering from ARMD. This is performed by using last stage.

Fusion of Fundus and OCT Analysis (Stage-3)

The proposed system comes to this stage once classification stages gives positive ARMD output for input OCT B-scan. For confirming whether or not the subject is suffering from ARMD, the proposed system correlates RPE analysis with the presence of drusens on the respective macular section in fundus image. In order to extract drusen patterns from macular region, the region of interest (ROI) across suspected OCT B-scan is extracted from fundus image. The system then detects possible drusens from this ROI by applying contrast enhancement using histogram equalization and OTSU thresholding algorithm as shown in Fig. 7 [45]. After applying an adaptive threshold based upon the computed probability mass function, a candidate fundus image is converted into a digital bitmap which depicts the extracted drusens. Here, a proposed system makes a decision out of two possible. If the RPE surface from OCT B-scan contains the presence of drusens while they are not appeared on fundus scan that indicate the early symptoms of the disease and system classifies it as suspect/early ARMD. However, if the drusen pathology is indicated in both imaging modalities then system classifies it as advanced ARMD. It confirms that the subject is suffering from ARMD syndrome and it needs immediate attention of specialists.

Table 5 Performance comparison of OCT, fundus, and fused systems using confusion matrices

OCT system	N	E	A	Fundus system	N	E	A	Fusion system	N	E	A
N	68	1	1	N	63	6	1	N	68	2	0
E	0	4	3	E	5	2	0	E	0	7	0
A	0	3	20	A	1	1	21	A	0	0	23
Accuracy (%)				Accuracy (%)				Accuracy (%)			
Normal, 97.14				Normal, 90				Normal, 97.14			
Early ARMD, 57.14				Early ARMD, 28.5				Early ARMD, 100			
Advanced ARMD, 86.95				Advanced ARMD, 91.3				Advanced ARMD, 100			

Results

The evaluation and testing of proposed system is carried out on locally developed dataset. The dataset has been acquired from AFIO and complete description about the dataset is given in Data Description section. For classifier training, we have used leave-one-out cross-validation technique during experimentations. To check the performance of fusion system, we have at first tested performance of OCT and fundus systems separately. For fundus image analysis, we have used our previously proposed technique published in [46]. Afterward, results generated by these two systems are compared with results generated by fusion system. Detailed analysis of proposed system is presented in Table 4. OCT image analysis is carried out at two levels. The data set was collected for 100 patients with 68 B-scans per patient. Table 4 shows that proposed technique for OCT image analysis achieves 96.4, 97.1, and 96.19% accuracy, sensitivity, and specificity, respectively at B-scan level. We further evaluated OCT analysis at patient level and this is carried out by analyzing 21 B-scans having fovea at center and overall output for specific patient is generated based on majority voting. This means that if most of B-scans out of these 21 are labeled as healthy by classifier then patient will be labeled as healthy else with ARMD.

Fundus image analysis on same dataset gives 86, 76.6, and 90% accuracy, sensitivity, and specificity, respectively. When we analyzed fused system having OCT and fundus image analysis both, then the results are same as we got with OCT analysis. It gives 98, 100, and 97.14% accuracy, sensitivity, and specificity, respectively. In Table 4, mentioned results apparently show no significance introduced by fusion technique. For this, we added detailed analysis for three classes, i.e., normal (N), early

ARMD (E), and advanced ARMD (A). Table 5 shows confusion matrices for OCT analysis, fundus analysis, and fusion analysis. Here, we added detailed results for three classes and evaluated OCT, fundus, and fusion analysis modules for three classes in hierarchal way. For OCT and fundus modules, SVM is used for binary classification, i.e., healthy and abnormal, and then at second level SVM is again used for classification of abnormal into early and advanced ARMD. In Table 5, an improvement can be seen in results generated by fusion system as compared to results that were generated by OCT and fundus systems separately. The fusion module detects changes in OCT scans for possibilities of ARMD signs and then it further goes for fundus analysis. Fundus image analysis has performed to classify early suspect and advance stage ARMD cases on the bases of drusen detection. If drusens are found in fundus image then its advanced ARMD, otherwise, is an early ARMD as there is no sign on fundus images; however, some are present in OCT image. It is clear from these confusion matrices, that proposed fusion of fundus and OCT scans enabled reliable grading of ARMD into early and advanced as compared to separate analysis of fundus images and OCT B-scans. The benefit of using fundus image analysis is that it helps to quantify area of drusens and helps to perform severity analysis of drusenoid region of ARMD affected patient's eyes that help ophthalmologists in diagnosis of ARMD stage and in further treatment of ARMD patient's. Figure 8 shows the RPE profiles of three randomly selected subjects from each category. The red color highlights the segmented ILM layer, green color indicates the segmented choroid, and yellow color highlights the segmented RPE layer. Apart from this, Fig. 9 shows the segmented drusens from the candidate fundus images. Drusens appearing on fundus images show the clear symptoms of ARMD syndromes. In the proposed system, we have used individual

Fig. 8 Segmented RPE profiles. **a** RPE profiles of healthy subjects. **b** RPE profiles of early ARMD patients **c** RPE profiles of severe ARMD patients
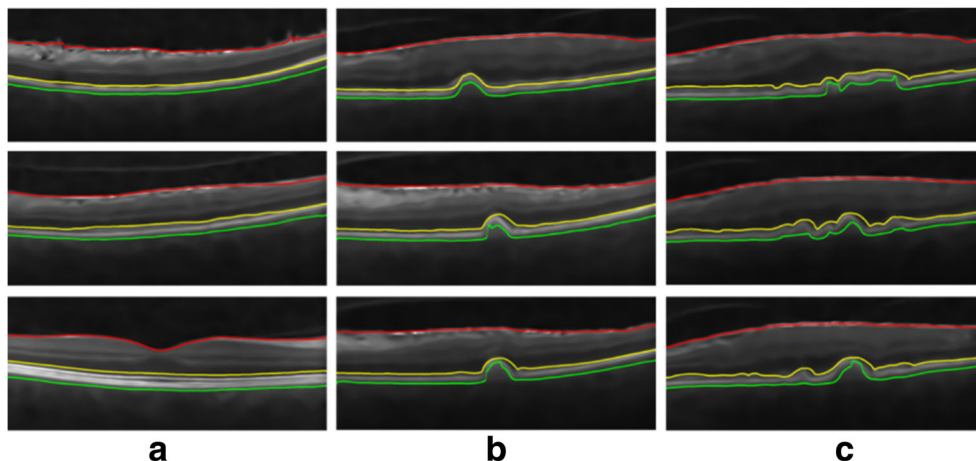
Fig. 9 Drusen extraction from fundus scans. Top row shows the extracted drusen from the respective fundus scans which are mapped onto the original images as depicted in the bottom row
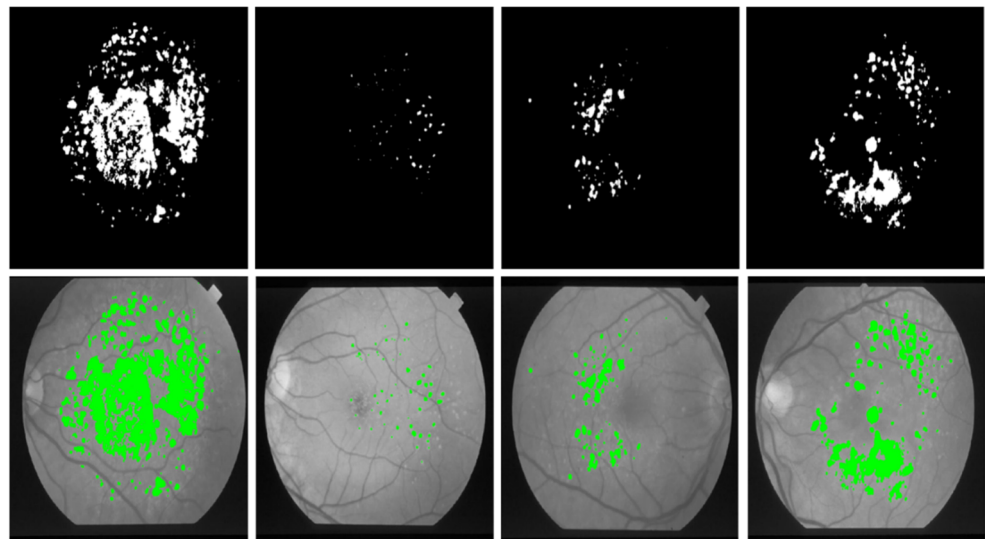
B-scans. However, the three dimensional visualization of OCT scans has a lot of clinical significance in detecting early signs as it gives the objective visualization of early ARMD pathological variations. Ophthalmologists also rely on 3D surfaces instead of single best selected OCT B-scan to diagnose retinal syndromes. This process of extraction of RPE layer as explained in RPE Layer Extraction (Stage-1) section is repeated for all the B-scans of a particular subject and all the extracted RPE profiles are then used to reconstruct a 3D retinal surface $R(x, y, z)$ as shown in Fig. 10.

Figure 11 shows the reconstructed RPE surfaces of three randomly selected subjects from each category in which RPE elevation gives a clear and objective indication of ARMD.

For this purpose, we have also constructed 3D surfaces from OCT imagery which can be part of decision support system.
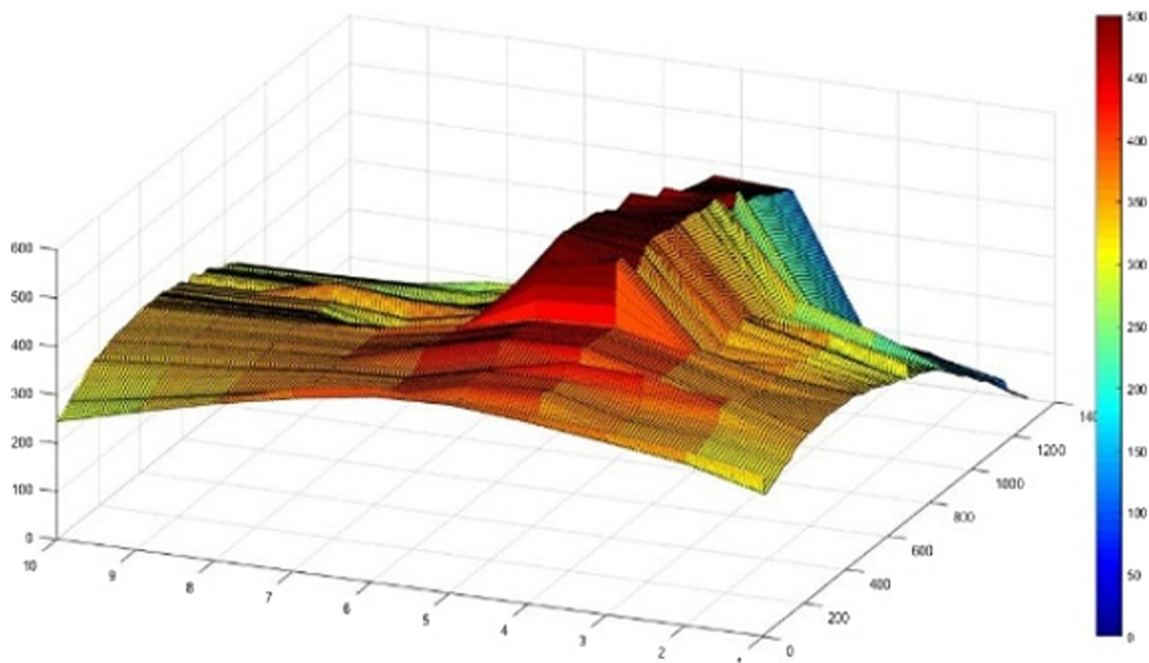
Fig. 10 Extracted RPE surface $R(x, y, z)$ to provide a 3D visualization of RPE
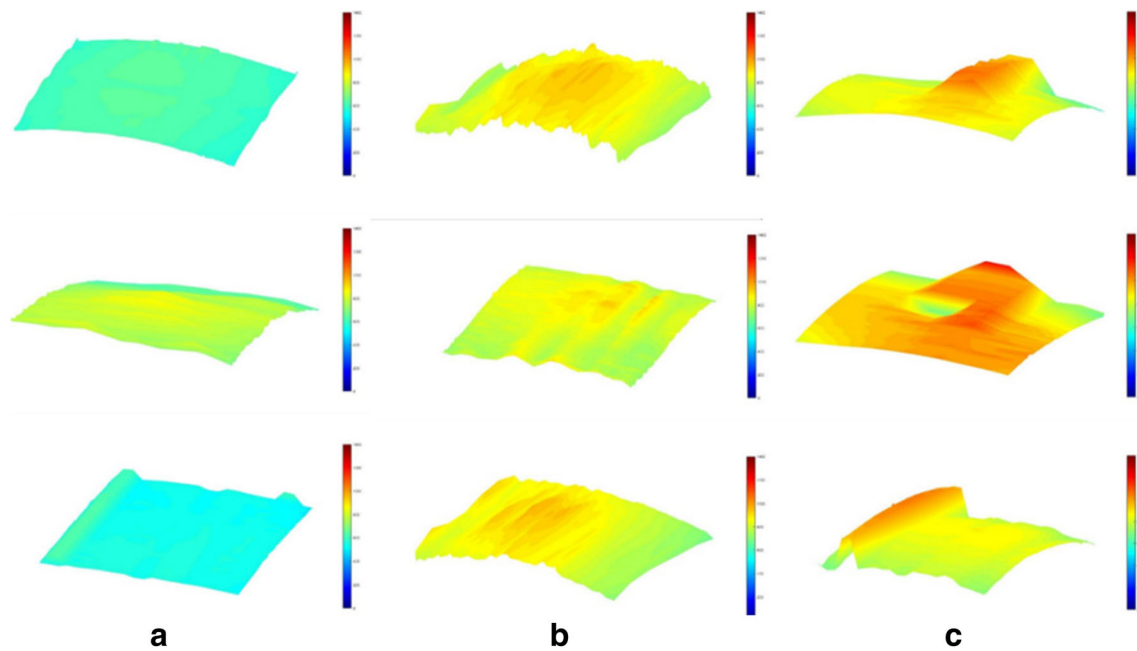
Fig. 11 Reconstructed RPE surfaces. **a** RPE surfaces of healthy subjects. **b** RPE surfaces of early ARMD patients. **c** RPE surfaces of severe ARMD affected subjects

Discussion and Conclusion

We proposed a fully autonomous system for detection of ARMD. The proposed system establishes a correspondence between OCT and fundus imagery to give accurate and reliable diagnosis of the ARMD disease. Five different features are extracted by the proposed system from OCT scans which are used to predict healthy and suspected ARMD subjects. The suspected ARMD subjects are further classified as having confirmed or early ARMD by extracting drusens in the respective macular region on the fundus image. It is worth noting that the proposed system is very robust in finding early disease patterns as shown in Fig. 12. Apart from this, proposed system establishes a correspondence between OCT and fundus imagery for
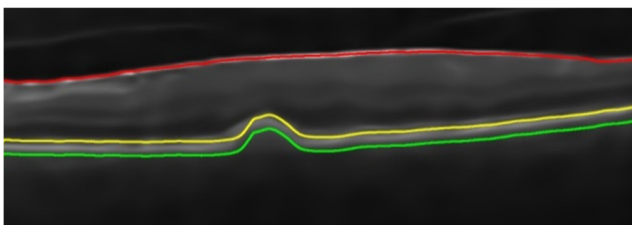
Fig. 12 Early symptoms of RPE atrophy due to the presence of drusen. This subject has been correctly identified by the proposed system

accurate and reliable detection of ARMD. The proposed system is also rotational invariant and it can accurately predict early ARMD cases from skewed OCT images. The classification system in the proposed method is based on supervised SVM classifier. First of all, the proposed classification system classify the subject as normal or early ARMD suspect by analyzing RPE atrophic surface. If the candidate is classified as suspect, then the proposed system further confirmed this as having early or advanced ARMD by measuring drusenoid area in the respective macular region of fundus image. The proposed system correctly classified a total of 98/100 subjects. The incorrect classification of two healthy samples as early diseased one is because we have tuned our system in such a way to give more priority to the ARMD samples because it is more critical to classify ARMD samples even its earliest stages accurately to be part of a telemedicine system. Our proposed system takes 57 s on average to give a complete disease diagnosis on a machine with fifth generation core i5 (2.2 GHz) and 4 GB DDR3 RAM.

We have also constructed 3D RPE surface by utilizing all B-scans of a patient. In future, this research can be extended for analysis of 3D RPE surfaces and grading ARMD into dry or wet as well as other macular and ocular syndromes like tractional retinal detachment (TRD), macular edema (ME), and glaucoma.

References

1. McHarg S, Brace N, Bishop PN, Clark SJ: Enrichment of Bruch's Membrane from Human Donor Eyes. J Vis Exp: JoVE 105:53382, 2015
2. "Age-related macular degeneration-EyeWiki", Eyewiki.aao.org, 2017. [Online]. Available: http://eyewiki.aao.org/Age related_macular_degeneration#Genetic_susceptibility. [Accessed: 02-Apr-2017]
3. Country Health Profile, World Health Organization, Retrieved: February 22, 2017.
4. Topouzis F, Anastasopoulos E, Augood C, Bentham GC et al.: Association of diabetes with age-related macular degeneration in the EUREYE study. Br J Opthalmol 93(8):1037–1041, 2009
5. Age related Macular Degeneration, National Eye Institute, Retrieved: February 22, 2017.
6. Brown MM, Brown GC, Stein JD, Roth Z, Campanella J, Beauchamp GR: Age-related macular degeneration: economic burden and value-based medicine analysis. Can J Ophthalmol/J Can Ophtalmol 40(3):277–287, 2005
7. Smith RT, Chan JK, Nagasaki T, Sparrow JR, Barbazetto I: A method of drusen measurement based on reconstruction of fundus background reflectance. Br J Ophthalmol 89(1):87–91, 2005
8. Srinivasan VJ, Wojtkowski M, Witkin AJ, Duker JS, Ko TH, Carvalho M, Schuman JS, Kowalczyk A, Fujimoto JG: High-definition and 3-dimensional imaging of macular pathologies with high-speed ultrahigh-resolution optical coherence tomography. Ophthalmology 113(11):2054–2065, 2006
9. Sbeh, Z.B., Cohen, L.D., Mimoun, G., Coscas, G. and Soubrane, G., 1997, October. An adaptive contrast method for segmentation of drusen. In Image Processing, 1997. Proceedings., International Conference on (Vol. 1, pp. 255–258). IEEE.
10. Rapantzikos, K. and Zervakis, M., 2001. Nonlinear enhancement and segmentation algorithm for detection of age-related macular degeneration (AMD) in human eye's retina. In Image Processing, 2001. Proceedings. 2001 International Conference on (Vol. 3, pp. 1055–1058). IEEE.
11. Rapantzikos K, Zervakis M, Balas K: Detection and segmentation of drusen deposits on human retina: Potential in the diagnosis of age-related macular degeneration. Med Image Anal 7(1):95–108, 2003
12. Thdibaoui, A., Rajn, A. and Bunel, P., 2000. A fuzzy logic approach to drusen detection in retinal angiographic images. In Pattern Recognition, 2000. Proceedings. 15th International Conference on (Vol. 4, pp. 748–751). IEEE.
13. Liang, Z., Wong, D.W., Liu, J., Chan, K.L. and Wong, T.Y., 2010, August. Towards automatic detection of age-related macular degeneration in retinal fundus images. In 2010 Annual International Conference of the IEEE Engineering in Medicine and Biology (pp. 4100–4103). IEEE.
14. Quellec G, Russell SR, Abràmoff MD: Optimal filter framework for automated, instantaneous detection of lesions in retinal images. IEEE Trans Med Imaging 30(2):523–533, 2011
15. Parvathi, S.S. and Devi, N., 2007, December. Automatic drusen detection from colour retinal images. In Conference on Computational Intelligence and Multimedia Applications, 2007. International Conference on (Vol. 2, pp. 377–381). IEEE.
16. Lee, N., Laine, A.F. and Smith, T.R., 2008, May. Learning non-homogenous textures and the unlearning problem with application to drusen detection in retinal images. In 2008 5th IEEE International Symposium on Biomedical Imaging: From Nano to Macro (pp. 1215–1218). IEEE.
17. Freund, D.E., Bressler, N. and Burlina, P., 2009, June. Automated detection of drusen in the macula. In 2009 I.E. International Symposium on Biomedical Imaging: From Nano to Macro (pp. 61–64). IEEE.
18. Brandon, L. and Hoover, A., 2003, November. Drusen detection in a retinal image using multi-level analysis. In International Conference on Medical Image Computing and Computer-Assisted Intervention (pp. 618–625). Springer Berlin Heidelberg.
19. Hassan, T., Akram, M.U., Hassan, B., Nasim, A. and Bazaz, S.A., 2015, September. Review of OCT and fundus images for detection of Macular Edema. In 2015 I.E. International Conference on Imaging Systems and Techniques (IST) (pp. 1–4). IEEE.
20. Abdelsalam A, Del Priore L, Zarbin MA: Drusen in Age-related macular degeneration: pathogenesis, natural course, and laser photocoagulation–induced regression. Surv Ophthalmol 44(1):1–29, 1999
21. Jain N, Farsiu S, Khanifar AA, Bearelly S, Smith RT, Izatt JA, Toth CA: Quantitative comparison of drusen segmented on SD-OCT versus drusen delineated on color fundus photographs. Invest Ophthalmol Vis Sci 51(10):4875–4883, 2010
22. Chiu SJ, Izatt JA, O'Connell RV, Winter KP, Toth CA, Farsiu S: Validated automatic segmentation of AMD pathology including drusen and geographic atrophy in SD-OCT images. Invest Ophthalmol Vis Sci 53(1):53–61, 2012
23. Farsiu S, Chiu SJ, O'Connell RV, Folgar FA, Yuan E, Izatt JA, Toth CA, Age-Related Eye Disease Study 2 Ancillary Spectral Domain Optical Coherence Tomography Study Group: Quantitative classification of eyes with and without intermediate age-related macular degeneration using optical coherence tomography. Ophthalmology 121(1):162–172, 2014
24. Huang D, Swanson EA, Lin CP, Schuman JS, Stinson WG, Chang W, Hee MR, Flotte T, Gregory K, Puliafito CA, Fujimoto JG: Optical coherence tomography. Science (New York, NY) 254(5035):1178, 1991
25. Fujimoto JG, Drexler W, Schuman JS, Hitzenberger CK: Optical Coherence Tomography (OCT) in ophthalmology: introduction. Opt Express 17(5):3978–3979, 2009
26. Srinivasan PP, Kim LA, Mettu PS, Cousins SW, Comer GM, Izatt JA, Farsiu S: Fully automated detection of diabetic macular edema and dry age-related macular degeneration from optical coherence tomography images. Biomed opt Express 5(10):3568–3577, 2014
27. Hee MR, Izatt JA, Swanson EA, Huang D, Schuman JS, Lin CP, Puliafito CA, Fujimoto JG: Optical coherence tomography of the human retina. Arch Ophthalmol 113(3):325–332, 1995
28. Lee JY, Chiu SJ, Srinivasan P, Izatt JA, Toth CA, Farsiu S, Jaffe GJ: Fully automatic software for quantification of retinal thickness and volume in eyes with diabetic macular edema from images acquired by Cirrus and Spectralis spectral domain optical coherence tomography machines. Invest Ophthalmol Vis Sci 54(12):7595–7602, 2013
29. Somfai GM, Tátrai E, Laurik L, Varga B, Ölvedy V, Jiang H, Wang J, Smiddy WE, Somogyi A, DeBuc DC: Automated classifiers for early detection and diagnosis of retinopathy in diabetic eyes. BMC Bioinf 15(1):1, 2014
30. Chen, Q., Leng, T., Kutzscher, L., Ma, J., Sisternes, L. D., Rubin, D. L., "Automated drusen segmentation and quantification in SD-OCT images", Medical Image Analysis, Vol 17, Issue 8, December 2013.

31. Fernández DC, Salinas HM, Puliafito CA: Automated detection of retinal layer structures on optical coherence tomography images. Opt Express 13(25):10200–10216, 2005

32. Chiu SJ, Li XT, Nicholas P, Toth CA, Izatt JA, Farsiu S: Automatic segmentation of seven retinal layers in SDOCT images congruent with expert manual segmentation. Opt Express 18(18):19413–19428, 2010

33. Bagci AM, Shahidi M, Ansari R, Blair M, Blair NP, Zelkha R: Thickness profiles of retinal layers by optical coherence tomography image segmentation. Am J Ophthalmol 146(5):679–687, 2008

34. Chiu SJ, Allingham MJ, Mettu PS, Cousins SW, Izatt JA, Farsiu S: Kernel regression based segmentation of optical coherence tomography images with diabetic macular edema. Biomed opt Express 6(4):1172–1194, 2015

35. Rossant, F., Ghorbel, I., Bloch, I., Paques, M. and Tick, S., 2009, June. Automated segmentation of retinal layers in OCT imaging and derived ophthalmic measures. In 2009 I.E. International Symposium on Biomedical Imaging: From Nano to Macro (pp. 1370–1373). IEEE.

36. Yang Q, Reisman CA, Wang Z, Fukuma Y, Hangai M, Yoshimura N, Tomidokoro A, Araie M, Raza AS, Hood DC, Chan K: Automated layer segmentation of macular OCT images using dual-scale gradient information. Opt Express 18(20):21293–21307, 2010

37. Yazdanpanah A, Hamarneh G, Smith BR, Sarunic MV: Segmentation of intra-retinal layers from optical coherence tomography images using an active contour approach. IEEE Trans Med Imaging 30(2):484–496, 2011

38. Wilkins GR, Houghton OM, Oldenburg AL: Automated segmentation of intraretinal cystoid fluid in optical coherence tomography. IEEE Trans Biomed Eng 59(4):1109–1114, 2012

39. Huang Y, Danis RP, Pak JW, Luo S, White J, Zhang X, Narkar A, Domalpally A: Development of a semi-automatic segmentation method for retinal OCT images tested in patients with diabetic macular edema. PLoS One 8(12):e82922, 2013

40. Kafieh R, Rabbani H, Kermani S: A review of algorithms for segmentation of optical coherence tomography from retina. J Med Signals Sens 3(1):45–60, 2013

41. Abhishek, A.M., Berendschot, T.T., Rao, S.V. and Dabir, S., 2014, December. Segmentation and analysis of retinal layers (ILM & RPE) in Optical Coherence Tomography images with Edema. In Biomedical Engineering and Sciences (IECBES), 2014 I.E. Conference on (pp. 204–209). IEEE.

42. Hassan B, Raja G, Hassan T, Akram MU: Structure tensor based automated detection of macular edema and central serous retinopathy using optical coherence tomography images. JOSA A 33(4):455–463, 2016

43. Syed AM, Hassan T, Akram MU, Naz S, Khalid S: Automated diagnosis of macular edema and central serous retinopathy through robust reconstruction of 3D retinal surfaces. Elsevier Comput Methods Programs Biomed 137:1–10, 2016

44. Cortes C, Vapnik V: Support vector machine. Mach Learn 20(3):273–297, 1995

45. Sezgin M: Survey over image thresholding techniques and quantitative performance evaluation. J Electron Imaging 13(1):146–168, 2004

46. Khalid, S., Akram, M. and Khalil, T. (2017) Hybrid textural feature set based automated diagnosis system for Age Related Macular Degeneration using fundus images. 2017 International Conference on Communication, Computing and Digital Systems (C-CODE)